Int. J. Solid Structures Vol. 18, No. 6, pp. 467–477, 1982.
Printed in Great Britain.

0020-7683/82/060467-11$03.00/0
Pergamon Press Ltd.

SHEAR AND NORMAL IMPACT LOADINGS ON ONE FACE OF A NARROW SLIT

L. M. BROCK
Department of Engineering Mechanics, University of Kentucky, Lexington, KY 40506, U.S.A.

(*Received* 10 *May* 1981)

Abstract—To gain insight into the transmission of impact load disturbances into elastic solids along narrow slits, the plane-strain problem of concentrated normal and shear forces applied suddenly to one face of a semi-infinite mathematical crack is treated. Exact solutions are obtained and the dynamic stress intensity factors and strain energy density intensity are studied. It is found that the dominant stress mode (I or II) near the crack edge changes rapidly with the arrival of the various waves from the concentrated forces. In particular, upon the Rayleigh wave arrival, the normal and shear forces cause, respectively, strong mode II and mode I behavior.

INTRODUCTION

The role of narrow cuts or slits as stress concentrators in elastic solids is well-known[1]. When the undeformed slit gap is vanishingly small (the slit is a mathematical crack) the stresses generated near the slit edge by the diffraction of incident waves may temporarily exceed the stresses for a corresponding quasi-static disturbance[2–5]. If the incident waves pass over the slit edge and then engulf the surfaces, the wave diffraction pattern in the crack limit arises, in effect, to remove the incident wave stresses which would occur on the slit surface region if no slit were present. However, the incident waves may reach the slit surface before arriving at the slit edge. In the crack limit the diffraction pattern now arises, in effect, to remove the displacement discontinuities which the incident waves would generate ahead of the slit region if the material were not joined there.

Such situations can arise when the disturbance generating the incident waves is on the slit surface itself; for instance, the slit may intersect an elastic solid surface subjected to impact loadings. With a view toward studying these situations, the present article considers the plane strain problem of concentrated normal and shear forces applied suddenly to one face of an initially undisturbed semi-infinite crack. The analysis is guided by [6], which considered the symmetric case of equal and opposite normal forces on either face. As in [6], particular attention focuses on the stress field near the crack edge.

As Lamb's problem analyses show[5, 7], even compressive loadings may produce temporary outward bulges on the surface to which they are applied. Since the undisturbed mathematical crack has no gap, this bulging implies material interpenetration. This difficulty can hypothetically be minimized or eliminated by superposing initial tensile stress fields which provide sufficiently large gaps. It can also be argued here that the crack is only a mathematical model of an actual slit with a small but finite gap. Moreover, while the loadings here are applied suddenly with arbitrary magnitudes, one goal of this work is to provide results which, by superposition, can be used for actual impact loadings. For these loadings, the bulging magnitudes are smaller than the finite gaps considered.

As seen in Fig. 1a, the crack is defined in terms of the Cartesian coordinates (x, y) by $y = 0$, $x < 0$. For $s = c_1 x(\text{time}) < 0$ the elastic solid is at rest, where (c_1, c_2) are the dilatational and rotational wave speeds. For $s > 0$ concentrated normal and shear forces N and S, i.e. line loads in the out-of-plane direction, are applied to the crack surface $y = 0^-$ at $x = -h$. Thus, along $y = 0$ we have

$$x < 0: (\sigma_y^+, \sigma_{xy}^+) = 0, (\sigma_y^-, \sigma_{xy}^-) = -(N, S)\delta(-x - h)H(s) \tag{1}$$

$$x > 0: (u^- - u^+, v^- - v^+) = 0 \tag{2}$$

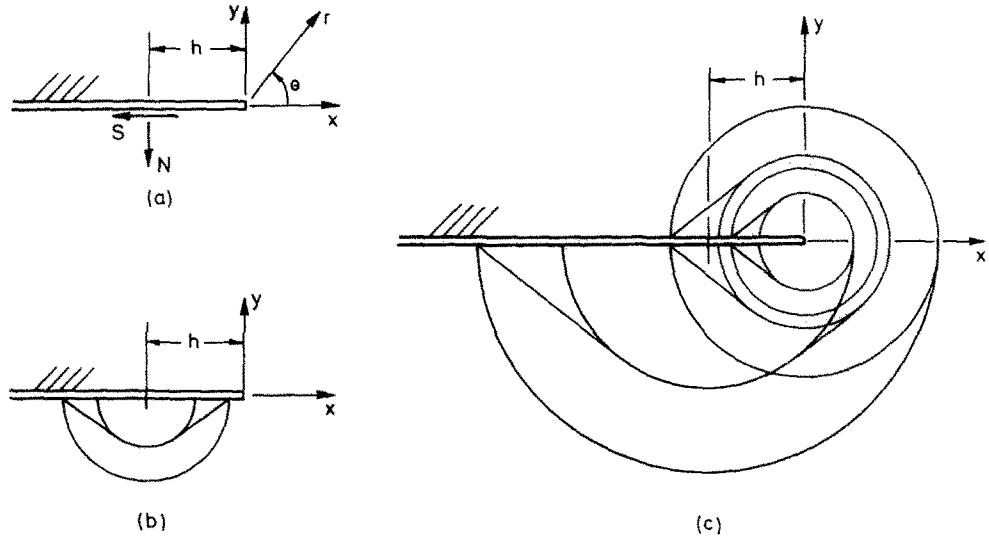

Fig. 1. (a) Loading and geometry, (b) Wave pattern for $0 < s < h$, (c) Wave pattern for $s > mh$.

where (u, v) are the displacements in the (x, y)-directions, δ and H are the Dirac and Heaviside functions and the superscripts denote field variables in the half-planes $\pm y > 0$. The governing equations in both half-planes are

$$\nabla^2(u, v) + (m^2 - 1)(u_{,x} + v_{,y})_{,(x,y)} = m^2(u, v)_{,ss}, \quad m = c_1/c_2 \tag{3}$$

$$\frac{1}{\mu}\sigma_x = m^2 v_{,y} + (m^2 - 2)u_{,x}, \quad \frac{1}{\mu}\sigma_y = m^2 u_{,x} + (m^2 - 2)v_{,y}, \quad \frac{1}{\mu}\sigma_{xy} = u_{,y} + v_{,x} \tag{4}$$

$$s \leq 0: (u, v) \equiv 0 \tag{5}$$

where μ is the shear modulus, $(\ )_{,a} \equiv \partial(\ )/\partial a$ and ∇^2 is the Laplacian operator.

When (N, S) are applied, a pattern of wavefronts radiates from the point $y = 0^-$, $x = -h$ into the half-plane $y < 0$. As seen in Fig. 1(b), this pattern defines the wave motion in the solid for $s < h$. For $s > h$ these waves reach the crack edge $(x, y) = 0$ and are diffracted. Figure 1(c) shows the wave pattern after the rotational wave has reached the edge $(s > mh)$.

Due to the characteristic length h, application of integral transforms directly to (1)–(5) leads to sectionally analytic functions in the transform space which are not related in a standard Wiener–Hopf manner [8]. This difficulty can be avoided by recognizing that if (2) is relaxed, the problem reduces to Lamb's problems [7] for two adjacent half-planes, where the loading on one half-plane vanishes. In view of the aforementioned property of the diffraction pattern, therefore, the original problem is essentially a superposition of the two Lamb's problems with the problem of displacement discontinuities prescribed across the plane ahead of an unloaded crack. In view of (2), these discontinuities are the negatives of the relative displacements of the two half-plane surfaces arising for $x > 0$ in the Lamb's problems. As in [6], the unloaded crack problem is itself constructed by a superposition of the basic solution treated in the next two sections.

BASIC SOLUTION

Consider the same crack with both surfaces now stress-free. At some instant $t = 0$ climb and glide dislocations of strength Δ_1 and Δ_2 appear at the crack edge and move in the positive x-direction with a constant speed cc_1. Equations (3)–(5) once again hold, with t replacing s, but (1) and (2) are replaced by

$$x < 0: (\sigma_y^{\pm}, \sigma_{xy}^{\pm}) = 0 \quad x > 0: (u^- - u^+, v^- - v^+) = (\Delta_1, \Delta_2)H(ct - x). \tag{6}$$

The Laplace transform over t and bilateral Laplace transform over x and its inverse are defined as [9]

$$f_L = \int_0^\infty f(t)\,e^{-pt}\,dt; \quad f_B = \int_{-\infty}^{\infty} f(x)\,e^{-pqx}\,dx, f(x) = \frac{P}{2\pi i}\int_\Gamma f_B\,e^{pqx}\,dq \tag{7a–c}$$

respectively, where p is real, positive and large enough to insure convergence of (7a), q is, in general, complex and Γ is the standard inversion path of integration. Application of (7a, b) in view of (5) and appropriate radiation conditions modify (3) and (4) merely by appending the superscripts $(\ )^* \equiv (\ )_{LB}$ and replacing the operators $(\ )_{,x}$ and $(\ )_{,s}$ with pq and p, respectively. Solutions to these transformed equations which are bounded for $\pm y > 0$ are

$$u^* = A^\pm e^{-pa|y|} + B^\pm e^{-pb|y|}, \quad \pm v^* = -\frac{a}{q}A^\pm e^{-pa|y|} + \frac{q}{b}B^\pm e^{-pb|y|} \tag{8}$$

$$a = a_+a_-, a_\pm = \sqrt{(1 \pm q)} \quad b = b_+b_-, b_\pm = \sqrt{(m \pm q)} \tag{9}$$

where $(A^\pm, B^\pm)$ are arbitrary functions of (p, q) and $(a_\pm, b_\pm)$ are defined in the q-plane cut along $\mathrm{Im}(q) = 0$, $\pm\mathrm{Re}(q) > (-1, -m)$ so that $\mathrm{Re}(a_\pm, a), \mathrm{Re}(b_\pm, b) \geq 0$. Application of (7a, b) to (6) gives

$$(\sigma_y^+ - \sigma_y^-, \sigma_{xy}^+ - \sigma_{xy}^-)^* = 0, \quad (u^- - u^+, v^- - v^+)^* = (\Delta U, \Delta V)^*, \quad (\sigma_y^+, \sigma_{xy}^+)^* = (\sigma, \tau)^* \tag{10a–c}$$

$$\Delta U^* = U^* + \frac{\Delta_2}{p^2(q+k)}, \quad \Delta V^* = V^* + \frac{\Delta_1}{p^2(q+k)} \tag{11}$$

along $y = 0$, where $k = 1/c$ and the Δ_i-terms exist as transforms for $\mathrm{Re}(q) > -k$. Here (σ, τ) and (U, V) are, respectively, the unknown stresses ahead of the crack edge and the unknown crack surface relative displacements. Thus, they vanish for $\pm x < 0$, respectively. Substitution of (8) into (10a, b) yields $(A^\pm, B^\pm)$ in terms of $(\Delta U, \Delta V)^*$, whereupon (10c) reduces to

$$\frac{\mu P}{m^2} R\left(\frac{1}{a}\Delta V^*, \frac{1}{b}\Delta U^*\right) = 2(\sigma, \tau)^*, \quad R = 4q^2ab + T^2, \quad T = m^2 - 2q^2. \tag{12a–c}$$

Here R is the Rayleigh function which exhibits simple zeros at $q = \pm n$, $n = c_1/c_R > m$ and c_R is the Rayleigh wave speed.

The quantities (σ, τ) and (U, V) radiate along $y = 0$ from the crack edge in, respectively, the positive and negative x-directions behind wavefronts defined by $t > \bar{k}x$ and $t > |x|$, where $\bar{k} = \min(k, 1)$. From (7a, b), then, the Laplace transforms of (σ, τ) and (U, V) behave as $e^{-p\bar{k}x}$ and $e^{-p|x|}$, so that $(\sigma, \tau)^*$ and $(U, V)^*$ exist in the overlapping half-planes $\mathrm{Re}(q) > -\bar{k}$ and $\mathrm{Re}(q) < 1$, respectively. Thus, the form of (12a) shows that, unlike the original problem, the basic problem reduces to two relations of the standard Wiener–Hopf type [8]. Because they are uncoupled, their solution is mathematically straightforward. Moreover, the uncoupling shows that the normal crack plane stress and relative displacement depend on the climb dislocation strength Δ_1, while the shear stress and tangential relative displacement on the crack plane depend on the glide dislocation strength Δ_2.

Study of (12b) shows that the function

$$G = \frac{R}{M(q^2 - n^2)}, \quad M = 2(1 - m^2) \tag{13}$$

is analytic in the strip $|\mathrm{Re}(q)| < 1$, has no zeros at $q = \pm n$ and approaches unity as $|q| \to \infty$. From analytic function theory [8], therefore, G can be written as the product of functions G_+ and G_-, where

$$\ln G_\pm(q) = -\frac{1}{\pi}\int_1^m \frac{1}{w \pm q}\tan^{-1}\left(\frac{4w^2b|a|}{T^2}\right)dw \tag{14}$$

which are analytic in the overlapping regions $\pm\mathrm{Re}(q) > -1$. Therefore, in view of (11) and the observations on $(\sigma, V)^*$, the first relation in (12a) can be rewritten as

$$\mu p \frac{M(q-n)}{m^2 a_-} G_- V^* + \frac{\mu}{p}\Delta_1 \frac{M}{m^2}\left(\frac{q-n}{q+k}\right)\frac{G_-}{a_-} = \frac{2a_+\sigma^*}{G_+(q+n)} \tag{15}$$

where the first term on the l.h.s. is analytic for $\mathrm{Re}(q) < 1$ while the r.h.s. is analytic for $\mathrm{Re}(q) > -\bar{k}$. The remaining term has a branch cut for $\mathrm{Im}(q) = 0$, $\mathrm{Re}(q) > 1$, a pole at $q = -k$ and behaves as $0(1/\sqrt{q})$ when $|q| \to \infty$. Therefore, from analytic function theory [8], it can be written as the sum of parts which are analytic, respectively, in the overlapping regions $\mathrm{Re}(q) < 1$ and $\mathrm{Re}(q) > -\bar{k}$. The splitting can be performed by inspection and (15) becomes

$$\mu p \frac{M(q-n)}{m^2 a_-} G_- V^* + \frac{\mu M}{pm^2}\frac{\Delta_1}{q+k}\left(\frac{q-n}{a_-} G_- + k_1\right) = \frac{2a_+\sigma^*}{G_+(q+n)} + \frac{\mu M}{pm^2}\frac{\Delta_1 k_1}{q+k} \tag{16}$$

$$k_1 = \frac{(k+n)G_+(k)}{a_+(k)}, \quad k_2 = \frac{(k+n)G_+(k)}{b_+(k)} \tag{17}$$

The r.h.s. and l.h.s. of (16) are clearly analytic in, respectively, the overlapping half-planes $\mathrm{Re}(q) > -\bar{k}$ and $\mathrm{Re}(q) < 1$. By analytic continuation, therefore, both sides represent the same entire function, say Z. Equations (6), (7a, b) and the fact that $V \equiv 0$ for $x > 0$ lead to the Abelian statement

$$v_L^-(0^-, 0) - v_L^+(0^-, 0) = \lim_{|q|\to\infty} pqV^* \tag{18}$$

where, in view of v's continuity at $(x, y) = 0$, the l.h.s. is Δ_1/p. Therefore, V^* must behave as $0(1/q)$, $|q| \to \infty$. Study of the l.h.s. of (16) then shows that we must have $Z \to 0$, $|q| \to \infty$ whereupon Liouville's theorem for bounded entire functions allows the conclusion $Z \equiv 0$. Equation (16) can now be solved for $(\sigma, V)^*$. A similar procedure is valid for the second relation in (12a). The expressions for $A^{\pm}$, $B^{\pm}$ now become

$$m^2 p^2 (q-n)(q+k) G_-(A^{\pm}, B^{\pm}) = \pm\left(q^2, \frac{T}{2}\right) b_- k_2 \Delta_2 + \left(-\frac{Tq}{2a}, qb\right) a_- k_1 \Delta_1 \tag{19}$$

and the basic problem is essentially solved. The transform inversion for the stresses and their behavior near the crack edge is illustrated in the next section, since this is required later.

STRESS BEHAVIOUR NEAR THE CRACK EDGE

As an example, we consider σ_y. For $y > 0$ eqns (5), (7), (8) and (19) give

$$\sigma_y^* = \frac{-\mu k_1 \Delta_1}{2m^2 p G_- a_+ (q-n)(q+k)}\left(T^2 e^{-pay} + 4q^2 ab\, e^{-pby}\right) + \frac{\mu k_2 \Delta_2 T q b_-}{m^2 p G_-(q-n)(q+k)}\left(e^{-pay} - e^{-pby}\right). \tag{20}$$

Substitution of the second k_2-term in (7c) yields

$$-\frac{\mu k_2 \Delta_2}{2\pi i m^2}\int_\Gamma \frac{Tqb_-}{(q-n)(q+k)G_-} e^{p(qx-by)}\, dq \tag{21}$$

where Γ can be taken as the $\mathrm{Im}(q)$-axis. Following the scheme of [10], the Cauchy theorem is used to change this path to a Cagniard contour along which $qx - by = -z$, where z is a positive, real parameter. Such a contour is readily found by solving this equation for q, so that (21) becomes

$$-\frac{\mu k_2 \Delta_2}{m^2 \pi}\int_{mr}^{\infty} \mathrm{Re}\left[\frac{Tqb_- b}{(q-n)(q+k)G_-}\right]\frac{e^{-pz}}{\sqrt{(z^2 - m^2 r^2)}}\, dz, \quad rq = -z\cos\theta + i|\sin\theta|\sqrt{(z^2 - m^2 r^2)} \tag{22a, b}$$

where $r = \sqrt{(x^2 + y^2)}$, $\tan\theta = y/x$ are the polar coordinates seen in Fig. 1. Equation (22b) defines one branch of a hyperbola with intercept $q = -m\cos\theta$. Appropriately, the hyperbola lies in the half of the q-plane where the exponential in (21) decays as $|q| \to \infty$. The Laplace transform of $\delta(t - z)$ is e^{-pz}, so clearly the inverse of (22a) is

$$-\frac{\mu k_2 \Delta_2}{m^2 \pi} \operatorname{Re}\left[\frac{Tqb_-b}{(q-n)(q+k)G_-}\right] \frac{H(t-mr)}{\sqrt{(t^2 - m^2 r^2)}} \tag{23}$$

where t replaces z in (22b). For $x < 0$, $m|\cos\theta| > 1$ the hyperbola intersects, and therefore must be deformed around, the branch cut $\operatorname{Im}(q) = 0$, $\operatorname{Re}(q) > 1$ of b_-/G_-. The integration along the additional contour gives, upon inversion, the extra contribution

$$-4M \frac{\mu k_2 \Delta_2 q^3 Tb_-b^2 (q+n) G_+ |a|}{m^2 \pi \, |R|^2 \sqrt{(m^2 r^2 - t^2)}} H(mr - t) H[t - rf(\theta)] \tag{24}$$

where, since G_+ is analytic for $\operatorname{Re}(q) > -1$, (13) has been employed and

$$rq = -t\cos\theta - \sin\theta\sqrt{(m^2 r^2 - t^2)}, \quad f(\theta) = |\cos\theta| + \sin\theta\sqrt{(m^2 - 1)}. \tag{25}$$

If $k < m$ it is possible that $m|\cos\theta| > k$, when for $x > 0$ the hyperbola crosses the simple pole at $q = -k$. The Cauchy residue theorem then gives yet another contribution which, upon inversion, becomes

$$\frac{\mu \Delta_2}{m^2} T(k) H[t - kx - b(k)y]. \tag{26}$$

Substitution of the first k_2-term in (20) into (7c) yields, similarly,

$$\frac{\mu k_2 \Delta_2}{m^2 \pi} \operatorname{Re}\left[\frac{Tqb_-a}{(q-n)(q+k)G_-}\right] \frac{H(t-r)}{\sqrt{(t^2 - r^2)}}, \quad rq = -t\cos\theta + i|\sin\theta|\sqrt{(t^2 - r^2)}. \tag{27a, b}$$

In this case, the hyperbolic Cagniard contour, of which (27b) defines one branch, does not intersect the branch cut of the integrand. Thus, no contribution analogous to (24) appears. If $k < 1$, however, it is possible that $|\cos\theta| > k$, when for $x > 0$ the simple pole at $q = -k$ is crossed, resulting in an additional contribution

$$-\frac{\mu \Delta_2}{m^2} T(k) H[t - kx - a(k)y]. \tag{28}$$

From a wave propagation viewpoint, (23) and (27a) define cylindrical rotational and dilatational waves which radiate from $(x, y) = 0$ while (24) describes head waves generated by coupling along the crack surface. The contributions (26) and (28) are the waves generated when the glide dislocation exceeds, respectively, the shear and dilatational wave speeds in the elastic solid.

To obtain the behavior of the k_2-contribution to σ_y near the crack edge for $y > 0$, we study (23)–(28) as $r \to 0$. For $t > 0$ (24), (26) and (28) give no contributions. However, when summed, (23) and (27a) behave as

$$-\frac{\mu M k_2 \Delta_2}{2\pi m^2} \frac{1}{\sqrt{(tr)}} \frac{1}{2} \sin\theta \cos\frac{3}{2}\theta. \tag{29}$$

A similar procedure for the k_1-contribution in (20) yields

$$-\frac{\mu M k_1 \Delta_1}{2\pi m^2} \frac{1}{\sqrt{(tr)}} \cos\frac{1}{2}\theta \left(1 + \sin\frac{1}{2}\theta \sin\frac{3}{2}\theta\right) \tag{30}$$

for $y > 0$, $r \to 0$. Results identical to (29) and (30) hold for $y < 0$, and their forms are similar to the corresponding expressions for the static problem [11, 12]. Results similar to (29) and (30) can be obtained for σ_x and σ_{xy}.

THE ORIGINAL PROBLEM

The solution for the Lamb's problems resulting from relaxing (2) can also be found by the transform methods involving (7a, b). The surface displacements for the half-plane $y<0$ are

$$\pi\mu u_L^- = \mp N\int_1 \frac{s}{X} q\,\mathrm{Im}\left(\frac{P}{R}\right)\mathrm{d}q + m^2 S\int_1 \frac{s}{X}\,\mathrm{Im}\left(\frac{b}{R}\right)\mathrm{d}q \tag{31}$$

$$\pi\mu v_L^- = m^2 N\int_1 \frac{s}{X}\,\mathrm{Im}\left(\frac{a}{R}\right)\mathrm{d}q \pm S\int_1 \frac{s}{X} q\,\mathrm{Im}\left(\frac{P}{R}\right)\mathrm{d}q \tag{32}$$

$$P = T - 2ab, \quad X = |x+h| \tag{33}$$

for $\pm(x+h)>0$ while clearly $u_L^+,\ v_L^+ = 0$. Here integration is along the lower side of the Re(q)-axis. As indicated previously, we wish to superpose upon the Lamb's problems the unloaded crack problem in which displacement discontinuities equal to the negatives of the relative surface displacements $u_L^- - u_L^+ = u_L^-$, $v_L^- - v_L^+ = v_L^-$ appear for $y=0$, $x>0$. Its solution can be generated from the basic solution as follows:

In the Lamb's problems, the first signals that (N, S) have been applied at $y=0^-$, $x=-h$ reach $(x, y)=0$ at $s=h$, as indicated by (31) and (32). Subsequently, the two half-plane surfaces for $x>0$ behave as if they were joined in the region $x>s-h$ but undergo the relative displacements (u_L^-, v_L^-) in the region $0<x<s-h$. Equations (31) and (32) show that $u_L^- = u_L^-(X/s)$ and $v_L^- = v_L^-(X/s)$, i.e. they are homogeneous functions of degree 0 in (X, s). Thus, the given values $u_L^-(X/s)$ and $v_L^-(X/s)$, in effect, travel along the x-axis with the constant speed $c_1 X/s$ $(s>0)$ which lies between zero and c_1. If cc_1 is a particular speed, then the corresponding values $u_L^-(c)$ and $v_L^-(c)$ reach $x=0$ at $s_0 = h/c$. Conversely, the speed with which these values reach $x=0$ at a given s is $c = h/s$.

Turning now to the basic solution, it is clear from the previous two sections that any scalar field variable has the form $\Delta_1 f_1(x, y, t, c) + \Delta_2 f_2(x, y, t, c)$. If the dislocations appear at $t_0>0$ instead of $t=0$ and the dislocation strengths are $-\mathrm{d}v_L^-(c)$ and $-\mathrm{d}u_L^-(c)$ instead of Δ_1 and Δ_2, then this form becomes $-f_1(x, y, t-t_0, c)\,\mathrm{d}v_L^-(c) - f_2(x, y, t-t_0, c)\,\mathrm{d}u_L^-(c)$, and can be summed over the range $h/s<c<1$. In view of the previous discussion, this weighted superposition of the basic solution gives the unloaded crack problem solution.

It follows that if (F, F_L, F_C) are corresponding scalar field variables for, respectively, the original, Lamb's and unloaded crack problems, then

$$F^\pm = F_L^\pm + F_C^\pm H(s-h), \quad F_L^+ \equiv 0 \tag{34}$$

$$F_C^\pm = \int_{h/s}^1 \left[f_1(x, y, t-t_0, c)\frac{\mathrm{d}v_L^-}{\mathrm{d}c}(c) + f_2(x, y, t-t_0, c)\frac{\mathrm{d}u_L^-}{\mathrm{d}c}(c)\right]\mathrm{d}c. \tag{35}$$

In (35) the expressions for $x+h>0$ are employed and, because t is measured from the time the dislocations appear at $x=0$,

$$t = s-h, \quad t_0 = h\left(\frac{1}{c}-1\right). \tag{36}$$

When $F^\pm = u^\pm$ along $y=0$, (34) shows that $u^+\equiv 0$, $u^- = u_L^-$ until the first signal from $y=0^-$, $x=-h$ reaches $x=0$ at $s=h$. Subsequently, $h/s<c<1$ and for $x>0$, eqn (6) and the uncoupling discussed in connection with (12a) guarantee that $f_1^- - f_1^+ = 0$, $f_2^- - f_2^+ = H[c(t-t_0)-x] = H(cs-x-h)$ for $u_C^\pm$. Thus, for $x>0$

$$u_C^- - u_C^+ = \int_{X/s}^1 \frac{\mathrm{d}u_L^-}{\mathrm{d}c}(c)\,\mathrm{d}c = -u_L^-(X/s), \quad u_L^- - u_L^+ = u_L^-(X/s) \tag{37}$$

and $u^- - u^+ = 0$, in accordance with (2). The analogous result holds for $v^\pm$, so that (35) apparently gives the solution to the original problem.

DYNAMIC STRESS INTENSITY FACTORS

In general, the Lamb's problem stresses are not singular at $r = 0$. Therefore, the behavior of σ_y as $r \to 0$ due to the normal relative displacement induced on the crack surfaces by (N, S) follows from (30), (32) and (35) as

$$-\frac{M}{2m^2\pi^2}\cos\frac{1}{2}\theta\left(1+\sin\frac{1}{2}\theta\sin\frac{3}{2}\theta\right)\frac{1}{\sqrt{r}}\int_{h/s}^{1}\frac{k_1}{\sqrt{(s-h/c)}}\left[Nm^2\,\mathrm{Im}\left(\frac{a}{R}\right)+\frac{S}{c}\,\mathrm{Im}\left(\frac{P}{R}\right)\right]\frac{\mathrm{d}c}{c^2} \quad (38)$$

where (a, P, R) are functions of $1/c$. In view of (17), therefore, it is convenient to introduce $k = 1/c$ as the integration variable, so that the integration in (38) becomes

$$-\frac{\mathrm{M}}{2m^2\pi^2\sqrt{h}}\int_1^{\tau}\frac{(k+n)G_+}{a_+\sqrt{(\tau-k)}}\left[Nm^2\,\mathrm{Im}\left(\frac{a}{R}\right)+Sk\,\mathrm{Im}\left(\frac{P}{R}\right)\right]\mathrm{d}k=\frac{1}{\pi}K_1(N,S) \quad (39)$$

where $\tau = s/h$ and integration is along the lower side of the Re(q)-axis. For $1 < \tau < m$ the integrations reduce to

$$\frac{2\pi m^2}{M}K_1(N,S)=\int_1^{\tau}\frac{(k+n)G_+P}{|R|^2\sqrt{(\tau-k)}}(PN-2bS)|a_-|\,\mathrm{d}k \quad (40)$$

while for $\tau > m$ the S-factor is modified by fixing the upper limit as m and adding the term

$$\frac{D(n)H(\tau-n)}{a_+(n)\sqrt{(\tau-n)}},\quad D(n)=\frac{\pi m^2 n}{MG_-(n)}[P(n)+2|a(n)||b(n)|] \quad (41)$$

and the N-factor is replaced by

$$\frac{\pi m^2}{\mathrm{M}}-\frac{\pi m^2}{\mathrm{M}}\frac{1}{G_-(n)}\sqrt{\left(\frac{n-1}{n-\tau}\right)}H(n-\tau). \quad (42)$$

The simple form of (42) follows from an integration of (39) by the Cauchy residue theorem; an analogous result was achieved in [6]. A similar procedure used with (29) gives the behavior of σ_y as $r \to 0$ due to the tangential relative displacement induced on the crack surfaces by (N, S). The total result is that as $r \to 0$,

$$\pi\sqrt{(hr)}\sigma_y \sim K_1\cos\frac{1}{2}\theta\left(1+\sin\frac{1}{2}\theta\sin\frac{3}{2}\theta\right)+\frac{1}{2}K_2\sin\theta\cos\frac{3}{2}\theta=K_y(N,S) \quad (43)$$

where for $1 < \tau < m$

$$\frac{\pi m^2}{M}K_2(N,S)=\int_1^{\tau}\frac{(k+n)G_+k}{|R|^2\sqrt{(\tau-k)}}(PN-2kbS)b_-|a|\,\mathrm{d}k. \quad (44)$$

For $\tau > m$ the N-factor is modified by fixing the upper limit as m and adding the term

$$\frac{D(n)}{b_+(n)}\frac{H(\tau-n)}{\sqrt{(\tau-n)}} \quad (45)$$

and the S-factor is replaced by

$$\frac{\pi m^2}{2M}-\frac{\pi m^2}{2M}\frac{1}{G_-(n)}\sqrt{\left(\frac{n-m}{n-\tau}\right)}H(n-\tau). \quad (46)$$

Relations similar to (43) can be derived for σ_x and σ_{xy}, where

$$K_x(N,S)=K_1\cos\frac{1}{2}\theta\left(1-\sin\frac{1}{2}\theta\sin\frac{3}{2}\theta\right)-K_2\sin\frac{1}{2}\theta\left(2+\cos\frac{1}{2}\theta\cos\frac{3}{2}\theta\right) \quad (47)$$

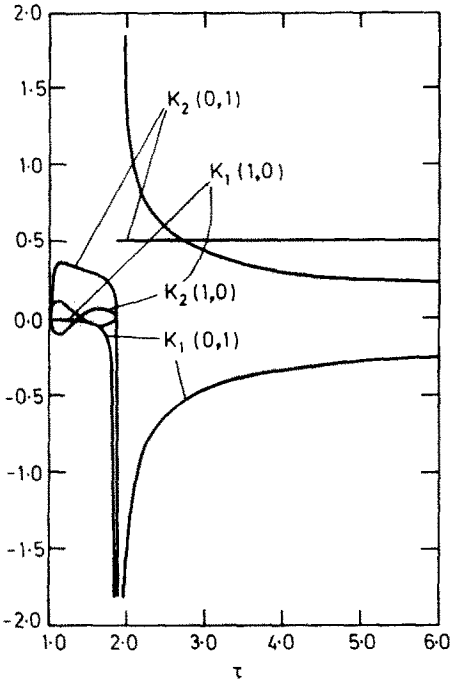

Fig. 2. K_1, K_2 vs τ.

$$K_{xy}(N, S) = \frac{1}{2}K_1 \sin\theta \cos\frac{3}{2}\theta + K_2 \cos\frac{1}{2}\theta\left(1 - \sin\frac{1}{2}\theta \sin\frac{3}{2}\theta\right). \tag{48}$$

The forms of (43), (47) and (48) show that $K_1/\sqrt{h}$ and $K_2/\sqrt{h}$ are essentially the mode I and mode II dynamic stress intensity factors. To examine their behavior, we study the cases of a unit normal ($N = 1$, $S = 0$) and unit shear ($N = 0$, $S = 1$) force. The parameters (K_1, K_2) are plotted vs τ in Fig. 2 for these cases when m takes the typical value $\sqrt{3}$. It is seen there that, in the first case, (K_1, K_2) grow continuously from zero when the first (dilatational) wave reaches the crack edge at $\tau = 1$. Until the Rayleigh wave arrival at $\tau = n$, K_2 is finite and changes sign while $K_1 < 0$ and square-root singular as $\tau \to n$. At the arrival, K_2 is square-root singular and then decays to zero as $\tau \to \infty$, while K_1 instantaneously takes the static value 0.5. This is half the static value for crack surfaces loaded by equal and opposite normal unit forces[6]. Thus, the crack edge is in compression until the Rayleigh wave arrival, but is in tension afterwards. From another viewpoint, K_1 and K_2 vie for dominance until just prior to the Rayleigh wave arrival. After the Rayleigh wave arrival, K_2 dominates K_1, but eventually the situation is reversed.

For the second case, Fig. 2 shows corresponding behavior with the roles of K_1 and K_2 reversed. However, the sign of K_2 indicates that, except for the interval just prior to the Rayleigh wave arrival, the crack edge shear stress and the direction of the unit force are consistent.

OTHER FRACTURE PARAMETERS

The mode I and mode II dynamic stress intensity factors often govern various criteria for brittle fracture initiation[12]. Fracture mechanics may also attempt to predict the direction in which fracture, once initiated, will proceed from the crack edge. Two criteria for this purpose assume that the crack will run in the direction of, respectively, maximum tensile stress[13] and minimum strain energy density intensity[14]. From (43), (47) and (48) the shear and normal stresses on planes radiating from the crack edge can for $r \to 0$ be written in polar coordinates as

$$\pi\sqrt{(rh)}\sigma_{r\theta} \sim \tfrac{1}{2}[K_1 \sin\theta + K_2(3\cos\theta - 1)]\cos\tfrac{1}{2}\theta = K_{r\theta}(N, S) \tag{49}$$

$$\pi\sqrt{(rh)}\sigma_{\theta} \sim (K_1 \cos\tfrac{1}{2}\theta - 3K_2 \sin\tfrac{1}{2}\theta)(\cos\tfrac{1}{2}\theta)^2 = K_{\theta}(N, S). \tag{50}$$

Here $K_{r\theta}/\sqrt{h}$ and $K_{\theta}/\sqrt{h}$ are dynamic intensity factors. Similarly, E, the strain energy density

per unit width normal to the xy-plane is given by

$$2\pi^2\mu rhE = \frac{m^2}{4(m^2-1)}(K_x - K_y)^2 + \frac{1}{m^2-1}K_xK_y + K_{xy}^2 = 2K_E(N, S) \tag{51}$$

as $r \to 0$, where $K_E/\mu h$ is the intensity. The parameters $(K_E, K_{r\theta}, K_\theta)$ are plotted vs θ in Figs. 3 and 4 for the two cases $(N = 1, S = 0)$ and $(N = 0, S = 1)$ at different values of $\tau > n$, where $m = \sqrt{3}$. Both figures indicate stationary value shifts with increasing τ.

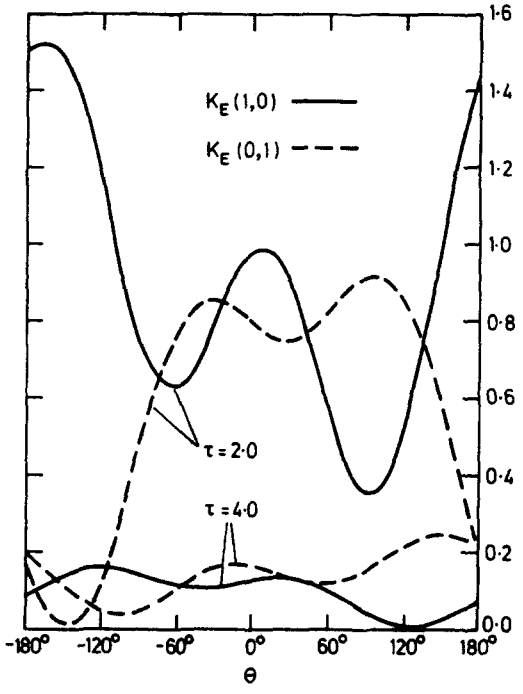

Fig. 3. K_E vs θ.

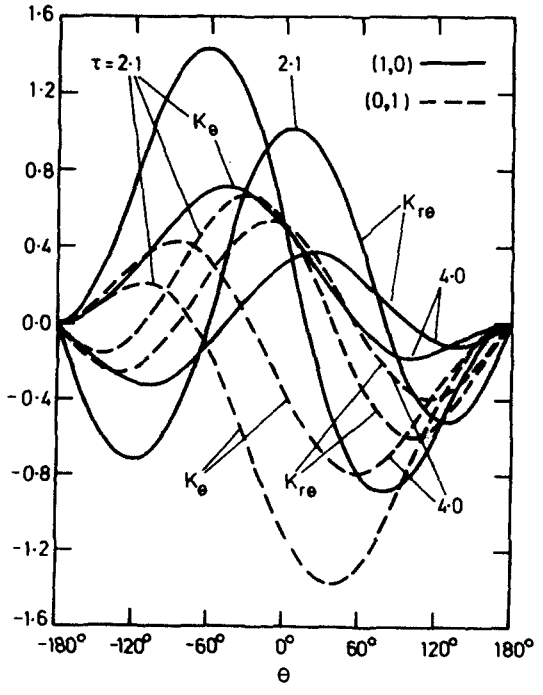

Fig. 4. $K_{r\theta}$, K_θ vs θ.

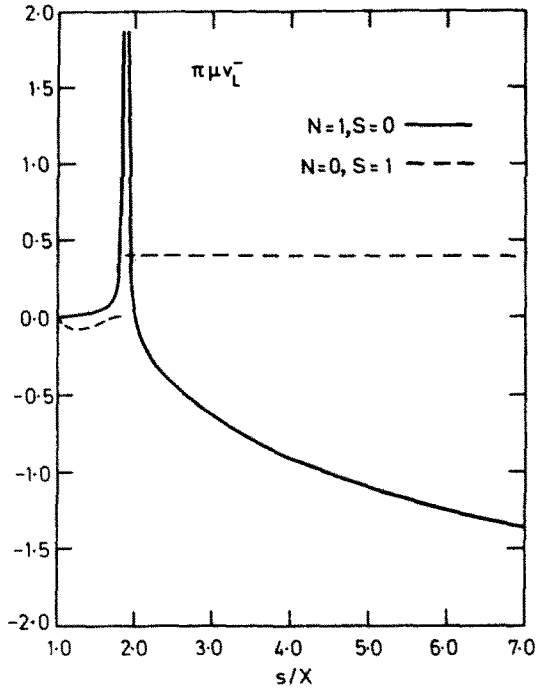

Fig. 5. $\pi\mu v_L^-$ vs s/X.

DISCUSSION OF RESULTS

In Fig. 5 the displacements $\pi\mu v_L^-$ are plotted for our two cases vs s/X when $x+h>0$ and $m=\sqrt{3}$. It is seen that the compressive force causes outward surface movement until the Rayleigh wave arrival, and inward movement subsequently. The shear force, however, causes the surface to move inward temporarily (outward when $x+h<0$). This behavior is consistent with the K_I response seen in Fig. 2. If, in view of (34), we take v_L^- as a measure, Fig. 5 shows that the surface bulging effect may be small except near the Rayleigh wave logarithmic peak due to the normal force. Thus, modeling a narrow slit as a mathematical crack may be a useful approximation, even for the severe impact loadings treated here. However, it should be noted that bulging effects may be important in cases where jagged surfaces can, in effect, mesh in gear-tooth fashion. Then, frictional effects and contact may have to be considered.

The results of the analysis presented here indicated that, until the Rayleigh wave arrival, the crack edge for either normal or shear concentrated forces is in a mixed-mode state complicated by the tendency of the crack surface to temporarily move in directions opposite to those of the corresponding forces. Just after the Rayleigh wave arrival, the normal and shear forces give rise to, respectively, mode II and mode I domination at the crack edge, while the corresponding modes take on their nominal static values. For long times, the corresponding modes do dominate, however. Then, except for a factor of 2, the stress state near the crack edge due to the normal (shear) force behaves as if the crack surfaces were symmetrically (antisymmetrically) loaded.

The solutions here were constructed by a superposing upon incident wave solutions a solution which applied the negatives of certain incident wave effects, thus defining a mathematical crack. In applying this approach to problems involving incident waves which first reach a crack at its edge [2–5], the crack plane stresses are the appropriate incident wave effects. Here, they were negatives of incident displacements. To construct the superposition-related problems, the approach of [6] was adopted and weighted dislocation solutions summed with respect to the dislocation velocity. This approach depended on the homogeneity (dynamic similarity) of the incident wave displacements. This approach can, of course, be used in other crack problems involving dynamically similar variables [15].

Acknowledgements—This problem was suggested by Dr. H. P. Rossmanith, Technische Universitat, Wien. The research was supported by the Department of Engineering Sciences, University of Oxford, and the Oxford University Computing Service.

REFERENCES

1. C. E. Inglis, Stresses in a plate due to the presence of cracks and sharp corners. *Trans. Instn. Naval Archit.* **55**, 219 (1913).
2. J. D. Achenbach, *Wave Propagation in Elastic Solids.* North-Holland, Amsterdam (1973).
3. L. M. Brock, Effects of secondary diffractions on the stress intensity factors generated for a finite crack by a shear wave. *Int. J. Engng Sci.* **13**, 851 (1975).
4. E. P. Chen and G. C. Sih, Scattering waves about stationary and moving cracks. *Elastodynamic Crack Problems* (Edited by G. C. Sih). Noordhoff, Leyden (1977).
5. J. Miklowitz, *The Theory of Elastic Waves and Waveguides.* North-Holland, Amsterdam (1978).
6. L. B. Freund, The stress intensity factor due to normal impact loading of the faces of a crack. *Int. J. Solids Structures* **12**, 179 (1974).
7. H. Lamb, On the propagation of tremors over the surface of an elastic solid. *Phil. Trans. Roy. Soc.* **A203**, 1 (1904).
8. B. Noble, *Methods Based on the Wiener-Hopf Technique.* Pergamon Press, Oxford (1958).
9. I. N. Sneddon, *The Use of Integral Transforms.* McGraw-Hill, New York (1972).
10. A. T. deHoop, A modification of Cagniard's method for solving seismic pulse problems. *Appl. Sci. Res.* **B8**, 349 (1960).
11. I. N. Sneddon and M. Lowengrub, *Crack Problems in the Classical Theory of Elasticity,* Wiley, New York (1969).
12. J. R. Rice, Mathematical analysis in the mechanics of fracture. *Fracture* (Edited by H. Liebowitz), Vol. II. Academic Press, New York (1968),
13. G. C. Sih and H. Liebowitz, Mathematical theories of brittle fracture. *Fracture* (Edited by H. Liebowitz), Vol. II. Academic Press, New York (1968).
14. M. E. Kipp and G. C. Sih, The strain energy density failure criterion applied to notched elastic solids. *Int. J. Solids Structures* **11**, 153 (1975).
15. P. Burgers and L. B. Freund, Dynamic growth of an edge crack in a half-space. *Int. J. Solids Structures* **16**, 265 (1980).